Vol. 36, No. 4 (2014) 394-405

Tribology in Industry

www.tribology.fink.rs

RESEARCH

Wear and Corrosion Resistance of Fe Based Coatings by HVOF Sprayed on Gray Cast-Iron for Automotive Application

M.S. Priyan[a], P. Hariharan[a]

[a]*Department of Manufacturing Engineering, College of Engineering, Anna University, India.*

Keywords:

Fe based coatings
HVOF
Characterization
Hardness
Wear
Abrasion
Corrosion

Corresponding author:

M. Shunmuga Priyan
Department of Manufacturing Engineering, College of Engineering, Anna University, India
E-mail: Shunceg@gmail.com

A B S T R A C T

In this study, commercially available FeSiNiCr and FeBCr alloy powders were designed with suitable compositions, gas atomized and then coated on gray cast-iron substrate. The microstructures of the feed stock Fe based alloy powders and the coatings were investigated by means of optical microscopy (OM), X-Ray diffraction (XRD), Thermogravimetric analysis (TGA) and Scanning Electron Microscopy (SEM). In the present study, both the coating materials experienced two-body wear mechanisms. The results showed that for loads of 0.05 N, 0.1 N and 0.2 N, the wear resistance of FeBCr coating was less than FeSiNiCr by 44 %, 40 % and 31 %, respectively. The results indicated that the coated substrates exhibited lower corrosion current densities and lower corrosion rates, when placed in 20 wt.% H_2SO_4 solutions. In addition, the use of optimal spraying parameters/conditions gave improvements to the corrosion resistance of the substrates that had been treated with the crystalline coating.

1. INTRODUCTION

The thermal spraying process is one of the most successful of all the advanced coating techniques because of the wide range of coating materials and substrates to which it can be applied. Metals and carbides are mostly used as coated materials, although spraying of polymers has also been researched [1,2]. Thermally sprayed coatings are used to protect components from different types of wear and corrosion [3-5]. The current field of the application of thermal spraying includes; the oil industry to protect component surface against hostile environment, automotive industry [6], and the space exploration industry Bowen et al (1992). In this literature reported in the Fe based alloy coating by HVOF process have appeared. Mostly Fe based metallic coating remains to form amorphous structure showing good adhesion to the substrate. However, it was found the $Fe_{43}Cr_{16}Mo_{16}C_{15}B_{10}$ metallic glass coating exhibited a very low co-efficient of friction under lubricating oil environment. Investigated FeCrSiBMn coatings prepared by high velocity oxy-fuel process on stainless steel [7]. Microstructures of the coating were investigated by the different techniques such as OM, SEM, and XRD.

The structure revealed the presence of Fe-Cr matrix and several kinds of borides. The form of amorphous and nanocrystalline grains exhibited in the structures in the shape of agglomerate powder materials. Investigated the coating of WC-CrC-Ni powder on substrate by HVOF process [8]. The author concluded that surface hardness depends on the parameters used in the coating process. The FeCrSiB alloy coating on stainless steel by HVOF process [9]. It was reported that the coated surface exhibited higher values of micro hardness because of molten and semi molten boride particle present in the microstructure and also due to the well flattened regions and un-molten particles. The studied NiCr coatings on stainless steel substrates and reported that the hardness values of the HVOF-sprayed coatings strongly depend on porosity, oxidized, un-melted/semi-melted particles [10], and inclusions. The coating of FeCrB based gas atomized powders, on steel substrates using the HVOF process [11]. The surface protective coatings resulted in superior corrosion/wear resistance, good magnetic properties and low material cost. The $Fe_{48}Cr_{15}Mo_{14}C_{15}B_6Y_2$ coatings on 316L stainless steel improved the corrosion resistance due to the proper proportion of porosity and amorphous fraction [12].

The HVOF sprayed coatings have been widely used for industrial applications where good wear or corrosion resistance are needed, because the coatings exhibits low porosity, high hardness, and low oxide content. The Fe-based amorphous metallic coatings on steel substrate can offer good corrosion resistance and mechanical properties such as high hardness, high strength and good abrasive wear resistance [13]. Fe-based metallic coatings can be employed in severe corrosive and/ or abrasive environments, and maybe replace hard chromium coatings in some special applications. Compared the corrosion resistance of FeCrMo–(C, B, P) amorphous coatings made by HVOF and APS processes on stainless steel substrate and reported that the corrosion potential of the amorphous coatings [14] sprayed by the HVOF process was higher and the passive current density was lower than that of the amorphous coatings sprayed by the APS process in 1N HCl solution. Reported that the amorphous form of $Fe_{43}Cr_{16}Mo_{16}C_{15}B_{10}$ alloy coating on steel substrates has been shown to have better corrosion resistance compared to the crystalline form in both 0.5M H_2SO_4 and 3.5 % NaCl [15].

The improved corrosion behaviour of the largely amorphous material is attributed to its homogeneity, and particularly to the elimination of the Mo-rich phase that underwent preferential corrosion in the crystalline form of the material. The FeSiBCCr coated on duplex stainless steel by using hard facing method. The microstructure had dispersed carbides of M7C3 in the cobalt rich FCC matrix [16]. The carbides provided the necessary abrasion resistance and corrosion resistance. Hardness at elevated temperatures is retained by the matrix. The efficiency of HVOF thermal spray coating of WC–Co powder on stainless steel and reported that the coating resulted in low porosity, better wear resistance, and superior hardness [17].

The wear mechanism has been mapped for a range of normal loads and volume fraction using diamond abrasive. Under dry sliding condition, HVOF sprayed Fe based alloy coating exhibit higher weight loss in this test duration at room temperature [18,19]. The performance of the structure of WC-12Co coating that is deposited on mild steel by high velocity oxy-fuel thermal spray process and reported that the coatings exhibit better abrasive resistance compared with conventional coating.

The present investigation of FeSiNiCr and FeBCr alloy powders on gray cast iron substrate by HVOF thermal spraying method under optimized conditions and to characterize the coated and uncoated specimens by various characterization techniques and also study the wear properties of coatings using diamond slurry abrasive wear testing. Further study the corrosion behavior of coated and uncoated specimen at sulphuric acid environment. Among the coatings, Fe-based amorphous coatings are more attractive due to their unique properties including high hardness, superior corrosion and wear resistance and relatively low cost. This paper presents work undertaken in the production of FeSiNiCr and FeBCr powders that were designed for use in thermal spraying. The powder feedstock and sprayed coatings have been micro-structurally characterised. The solid coatings were subjected to diamond slurry abrasive wear testing. In addition, the mechanism of corrosion testing on both materials was examined.

2. EXPERIMENTAL DETAILS

2.1 Powder Raw Materials

The commercially available gas atomized FeSiNiCr and FeBCr powders were chosen in this work. The raw material for the coating, namely the FeSiNiCr alloy powder, was obtained from M/s L&T EWAC powders Ltd. The atomized Fe-based alloy powders, with an average particle size in the range of 15-50 μm were used for spraying onto the gray cast-iron substrates. Powders of the same composition were produced by a high pressure argon gas atomization method. They were then sieved according to conventional sieve analysis, being subdivided into different size ranges.

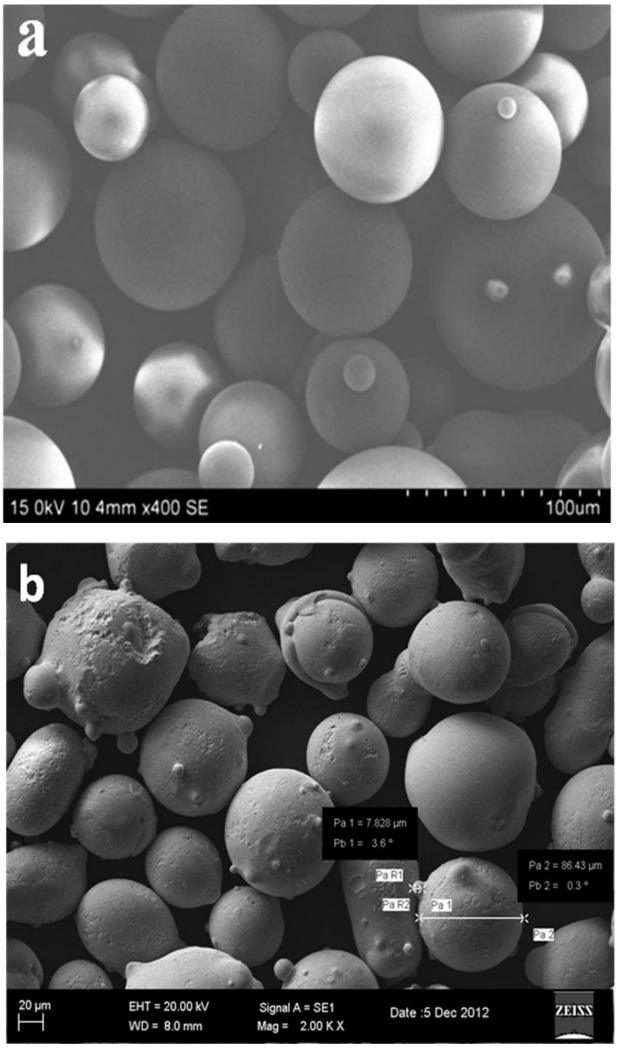

Fig. 1. SEM micrographs of (a) FeSiNiCr powder, (b) FeBCr powder.

The particle size distributions of the un-agglomerated feedstock fractions (15 μm < size < 50 μm) and (size < 75 μm) of powders A and B were measured using a laser particle size analyzer (Malvern Mastersizer). The particle size distributions of the PVA-agglomerated feedstock fractions were measured using SEM images. The SEM image of FeSiNiCr powder is shown in Fig. 1. The average size of the particle is in the range of 25–45 μm. The majority of the particles that were produced by gas atomization in argon atmosphere are spherical or near-spherical although some have small satellites attached. Most of the particles exhibit a smooth surface, thus, being the source of the good fluidity of the system.

2.2 Substrate Preparation

Gray cast iron was considered as the desired choice of substrate material, because of being its wide application in automotive field continuous abrasion and exposure to high temperature is undergone in its regular service. The chemical composition of the selected substrate material and coating powders composition is provided in Table 1.

Table 1. Chemical composition of the substrate and coatings.

Comp (Wt. %)	Fe	C	B	Si	S	Cr	Mn	Ni	P
Gray cast-iron	94	3.0	1.8	1.32	0.28	0.08	0.26	0.01	0.28
Fe SiNiCr	73	-	-	15	-	02	-	10	-
FeBCr	59	-	26	-	-	15	-	-	-

Table 2. HVOF process parameters.

SI. No	Parameters	Qty
1	Gun type (Super jet Gun)	1 No
2	Pressure of Oxygen	2.5 Kg/cm^2
3	Pressure of acetylene	0.6 Kg/cm^2
4	Torch angle with respect to substrate	60°
5	Torch Speed	12 cm/min
6	Distance of torch tip from the substrate	25 mm
7	Preheat temperature	200 °C
8	Post spray heat treatment temperature	800 °C

Suitable specimens, (length 12 mm and diameter 24mm), were fabricated from the substrate bar by EDM wire cutting to a close proximity to the required size, followed by the grinding of both the faces to remove surface irregularities as well as to deal with the consequences of any induced micro-level changes that might have occurred in the heat affected zone as a result of the EDM cutting. The surface roughness of the samples was maintained at around 0.6μm by the grinding operation. The operating parameters of the spray system for deposition of the coating types are illustrated in Table 2.

2.3 Coating Characterization Methods

Samples from the surfaces of the coatings and from cross sections of the coatings were polished using a series of coarser to finer grades of silicon carbide emery papers and then finally polished with a diamond paste, applied on a velvet cloth that was attached to a rotating disc. In this way, micro-polished surfaces were obtained for further analysis and evaluation. Scanning Electron Microscopy (SEM) image analysis was used to quantify the distribution of different phases in the samples of interest. Optical microscopy was used to calculate porosity level by image analysis. The coating thickness values were determined by the SEM technique using the cross sectioned samples. A stereographic image analysis system was employed to estimate the average porosity (%) of the coated surface, by analyzing and averaging various optical micrographs that were taken at different surface regions of the coating, as outlined in the standard test method, ASTM B276. To give a guide to the weight percentage of particular elements and atoms, EDAX was used at random locations on the coating surface. Also X-Ray Diffraction (XRD) patterns were used to characterize the coating type. This XRD analysis of the specimens was performed on an X-ray diffractometer (Cu K_α radiation) with a range of 2θ diffraction angles from 40 to 50°. The micro-hardness value was determined for the uncoated specimens and for the coated specimens. The micro-hardness was tested at various places on the coating surface using Wolpert Wilson equipment, model 402 MVD. A load of 1 N (100 g) was employed for a dwell time of 10 seconds. Simultaneous thermogravimetry-differential analysis (TG-DTA), in air, (10 °C/min heating rate up to 1000 °C) was performed on the coated specimen.

2.4 Wear test and evaluation

Wear performance of the coating vis-à-vis the bare substrate was assessed by a micro abrasion test in which the samples were subjected to a block-on-ring method of testing with diamond slurry as abrasive medium to increase the severity of the abrasion. A commercially available Wear and friction unit (Tech. (India) Pvt Ltd), Fig. 2 was used for the test, in accordance with the standard ASTM G 77 procedures, in which the coated samples were pressed against a directly driven steel ball, under a fixed load, rotating at 150 revs/minute corresponding to a linear sliding distance of 11.78 m.

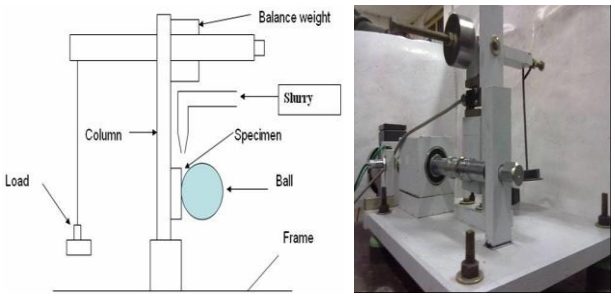

Fig. 2. Schematic diagram of micro-abrasion tester.

Table 3. Micro-abrasion test parameters.

Substrate	FeSiNiCr alloy coated specimen, Surface roughness R_a= 0.6μm. Specimen dimension (12 mm length and 24 mm diameter)
Ball material	High Carbon – High Chromium material conforming to EN 31 Ball diameter-25.4 mm, Surface roughness R_a=0.068μm. Hardness -750 VHN at 100g load.
Sliding distance	24, 48 and 72 m
Load	0.05, 0.1 and 0.2 N
Slurry	Diamond slurry with distilled water, Particle size (<1μm) triangular shape

The test sample was clamped onto a platform, fitted to the pivoted L-shaped arm. This arm was rotated around its pivot until the sample became in contact with the ball. The beam was in balance when the samples were in contact and the load was applied by adding dead weights to a cantilever arm. This configuration has the advantage of providing accurate control of both the normal load and the sliding speed. Furthermore, the coating was subjected to abrasion testing using three different loads, namely 0.05, 0.1, and 0.2 N, for durations of 2, 4, and 6 minutes for each of these loads. Diamond powder-based slurry was continuously fed onto

the interface between the ball and sample throughout the tests. The complete test parameters are presented in Table 3.

2.5. Electrochemical evaluation

The electrochemical corrosion behaviour of the uncoated, gray cast iron and of the iron-alloy coated gray cast iron was evaluated in 20 wt.% H_2SO_4 solution, at ambient temperature, using a potentiostat model (PGSTAT model 12, AUTOLAB, The Netherlands BV) controlled by a personal computer. A conventional, three electrode cell, containing 200±2 mL of electrolyte was equipped with the substrate as the working electrode (1 cm^2). Platinum foil and a saturated calomel electrode (SCE) were used as the counter electrode and the reference electrodes respectively. The substrate was exposed to the H_2SO_4 solution for about 45 minutes to establish the open circuit potential (E_{OCP}). The change in open circuit potential (OCP) was monitored and presented as a potential versus time plot. The system was then allowed to attain a constant open circuit potential and the electrode polarized from -0.8 to 0.2 V, with a scan rate of 1 mV/s. The polarization plots obtained are depicted as the potential vs. log i plot.

3. RESULTS AND DISCUSSION

3.1 Microstructure of FeSiNiCr and FeBCr Coatings

The optical microscopy was used to study of the microstructure of the FeSiNiCr and FeBCr alloy coated specimens. The amount of porosity of the coatings was evaluated by image analysis by optical microscopy on polished cross sections. The porosity results of the coated surface are less than 1 % reported by analyzing and averaging various optical micrographs taken at different areas of the coating as outlined in the standard test method, ASTM B276. Figure 3 depicts the optical micrograph of the top surface of the coating. It indicates a uniformly distributed fine-grained microstructure. It shows fine grained and homogeneous structure coated specimen. It is concluded that the optical micrograph (Fig. 4) of the FeBCr alloy coating is less porous than the FeSiNiCr alloy coated specimen. The grains of FeBCr coating are found to the finer size than FeSiNiCr coating. Microstructure of surface and cross section are identical, shown in Fig.3, and is replete with uniformly distributed fine grains like powder deposits with prominent wide boundaries, suggesting a consistent coating through HVOF process.

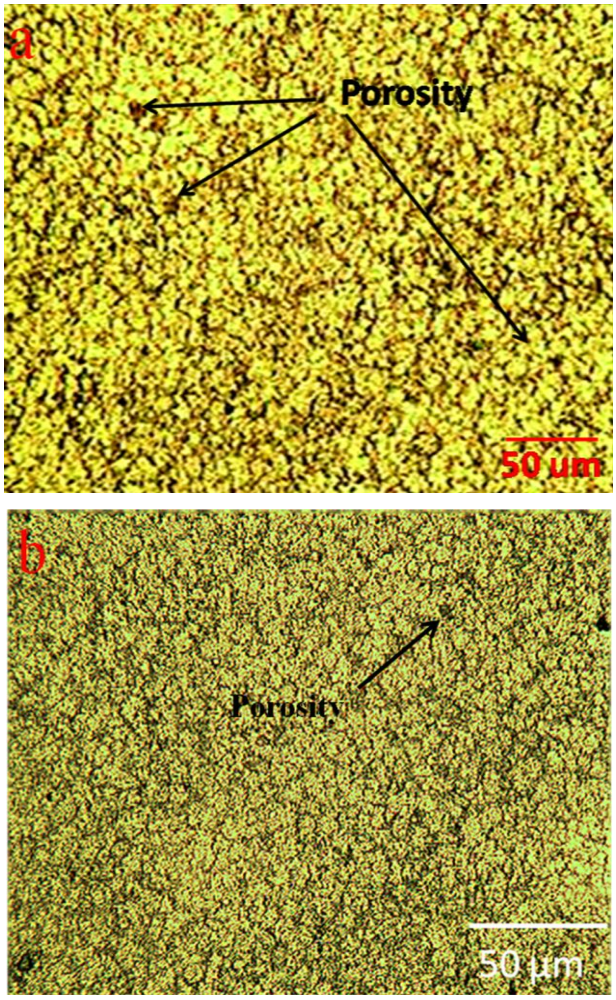

Fig. 3. Optical micrographs showing surface morphology of (a) FeSiNiCr coated specimen, (b) FeBCr coated specimen.

SEM study on the cross section sample implies a consistent coating with an average coating thickness of 400 µm. Intricate features like gaps, cavities and boundaries in between the deposits are more clearly visible in the SEM images, which shown in Fig. 4. The molten powders on impinging the substrate have flattened and solidified separately in to splats that are evenly distributed and at the same time randomly laid over one another, leaving numerous gaps and separations in between the splats. Despite this coating anomaly which is an inherent feature, the overall porosity is less than 1.5 % and more

over same level of porosity persists throughout the coating, signifying a good deposition and better process control. The formation of a dense coating is attributed to the high velocity of impinging that is the characteristic of HVOF process.

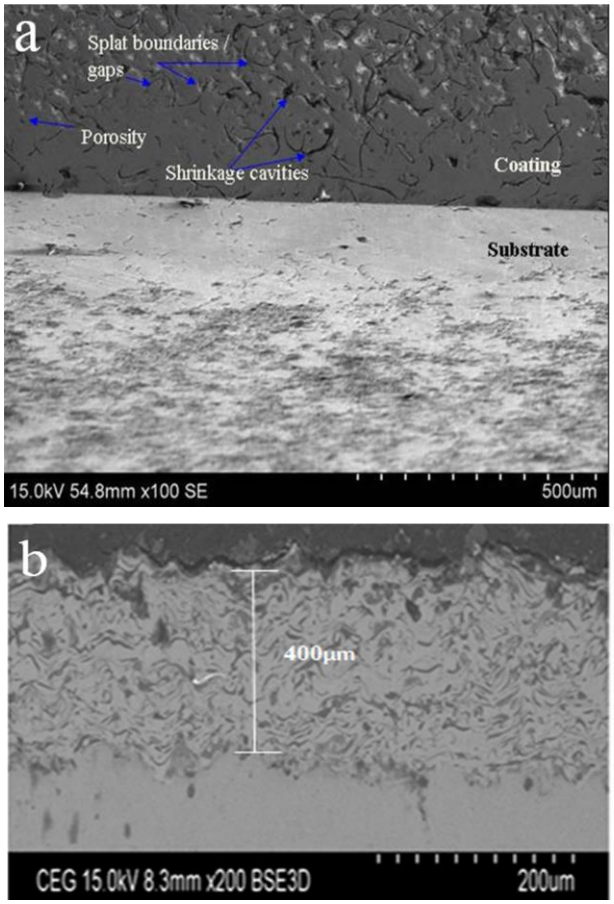

Fig. 4. SEM image of the cross section of (a) FeSiNiCr alloy coating, (b) FeBCr alloy coating.

3.2 Micro Hardness of the FeSiNiCr and FeBCr Coatings

Micro hardness profile along the cross section of the coating as a function of distance from the coating–substrate interface is shown in Figure 5, from which it is observed that there is a gradual increase of hardness from the interface towards the coating surface. The average surface hardness of coating is 920 HV, about twice that of the substrate hardness which is around 350 to 400 HV. Towards the interface the coating hardness is around 750 HV and at a distance of 250 microns above the interface, the hardness reaches a maximum level of about 910 HV and remains stabilized up to the surface at 450 µm away from the interface. Stabilized hardness is of high significance as it enhances the wear resistant capabilities of the coating compared to a gradient hardness. High hardness of the coating is attributed to the solid solution strengthening by Ni and Cr in Fe phase. From Fig. 5 it is concluded that FeBCr alloy coating hardness is 6.5 % higher than FeSiNiCr alloy coated specimen. The high hardness and the absence of grain boundaries lead to better resistance to the wear of the coated specimen. In addition, the coating has very dense structure and lower porosity.

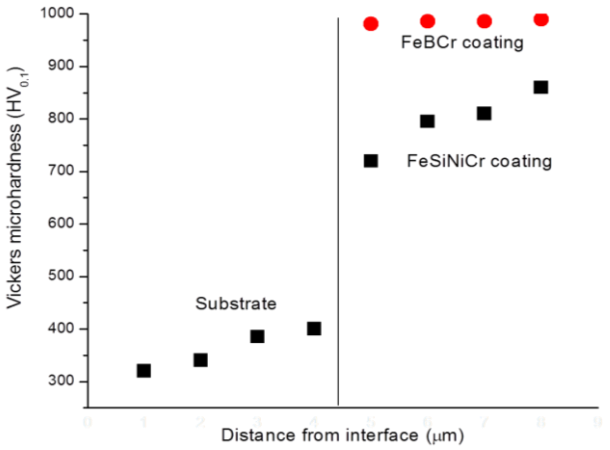

Fig. 5.Micro hardness profile for FeSiNiCr and FeBCr alloy coated with substrate specimen

3.3 X-ray diffraction analysis of FeSiNiCr and FeBCr coatings

The XRD patterns of the atomized powder, substrate material and deposited of coating are shown in Fig. 6. Figure confirms the coating to be predominantly of a crystalline nature, as seen in the sharp peak corresponding to the α phase, at 2θ, of 45°.

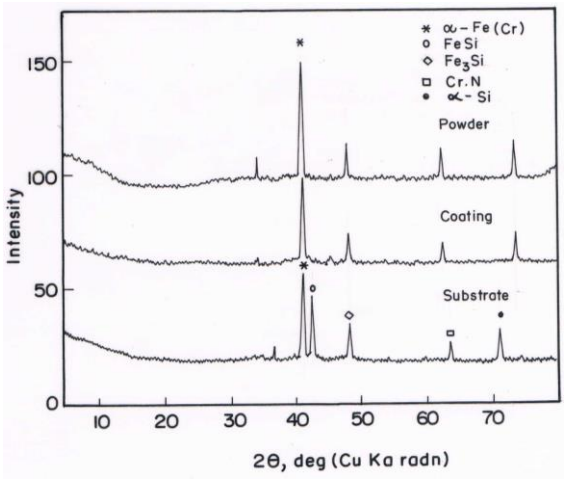

Fig. 6. XRD pattern of FeSiNiCr-based powder with coating.

With the FeSi alloy, the X-ray patterns showed that coating structures are more crystalline than the structure of powder and that the cubic structure of Fe_3Si is the principal characteristic of the FeSi alloy, Fig. 6. These results are similar to those obtained by the rapid quenching of FeSi mechanically produced alloys. The diffraction pattern confirms the BCC structure of the α-Fe matrix. It is worth noting the emergence of a broad halo between the 2θ values of approximately 40° and 60°. These are related to the formation of a crystalline phase. XRD pattern of FeBCr coating is shown in Fig. 7.

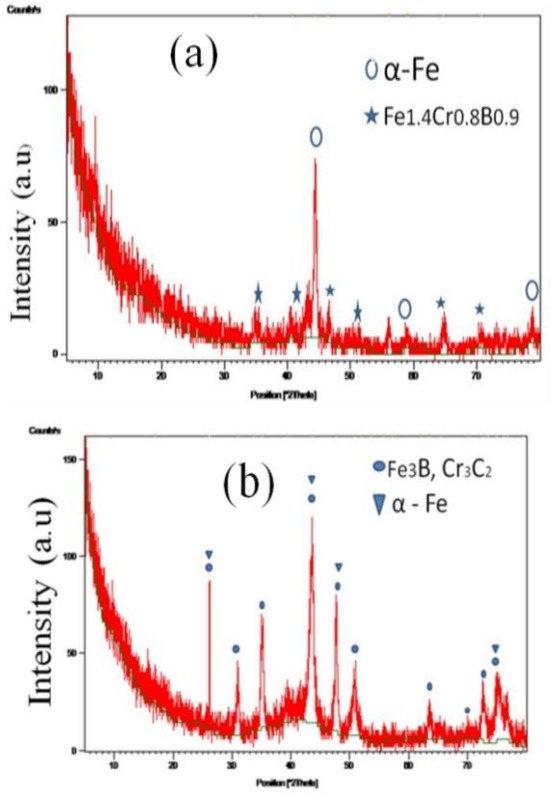

Fig. 7. XRD pattern of (a) FeBCr alloy powder (b) FeBCr coated Specimen.

From the X-ray pattern more crystalline structure is formed in the coated specimen at ambient condition. Some sharp diffraction peaks appearing at 2θ = 45° and 52.5° indicate the presence of a crystalline phase. However, the sharp peaks due to crystalline phases are also observed. The major crystalline phases are compounds Fe_3B, and solidification α-Fe (Cr). It is observed from Fig. 7 that the FeBCr coated peaks of Cr_3C_2 are less sharp, which implies the increasing in ability of the formation of the crystalline phase. These results are similar to those obtained by the rapid quenching of FeB mechanically produced alloys. The diffraction pattern confirms the BCC structure of the α-Fe matrix.

3.4 Wear Rate Performance of FeSiNiCr and FeBCr Coated Specimens

The wear rate performance of FeSiNiCr and FeBCr coating measured under 0.05 N is shown in Fig. 8.

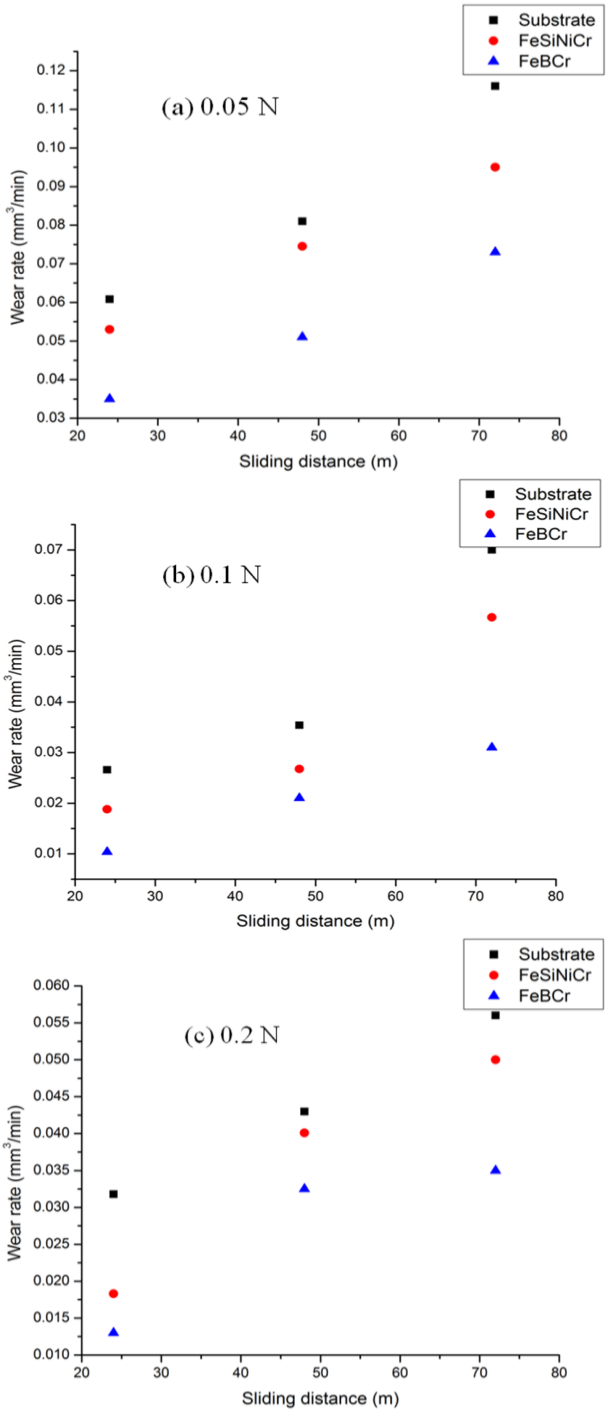

Fig. 8. Wear rate in sliding distance, for normal load applied on harden surfaces function of time (a) 0.05 N (b) 0.1 N (C) 0.2 N.

The mechanism of wear and the resulting wear rate depend strongly on the ratio of the hardness of the abrasive particles to that of the binder phase. Another way of judging the wear performance is to compare the extent of material removal in terms of wear volume, in both the coating and the substrate. From the direct plot of the wear rate and the test time, Fig. 8, it is apparent that the volume of wear increases as the applied load increases and as the testing duration increases. As expected, under each load condition, the coating exhibits comparatively less wear than the substrate. Interestingly, the wear performance of the coating is nearly 80 % greater than that of the substrate, at a 0.05 N applied load. However, at the greater applied loads of 0.1 N and 0.2 N, the wear performance of the coating declines more drastically, being only slightly better, by about 20 % and 15 % respectively, than the wear performance of the substrate. Thus, above the 0.05 N load, the coating performs with consistently less wear resistance. The wear rate resulted of FeSiNiCr coating, almost 8 %, 26 % and 22 % reduction in wear rate was observed under 0.05 N, 0.1 N and 0.2 N loads respectively. Similarly, in the FeBCr coating, almost 36 %, 47 % and 41 % reduction in wear rate was observed under 0.05 N, 0.1 N and 0.2 N loads respectively.

3.5 Co-efficient of Friction of FeSiNiCr and FeBCr Coatings

Co-efficient of friction FeSiNiCr and FeBCr coating measured under 0.05 N is shown in Fig. 9. The friction co-efficient of the crystalline coatings and of the gray cast iron substrates, related to testing time, was monitored. Wear tests were performed on the surface of the coated material as well as on the un-coated substrate to evaluate the effect of the surface coating on the nominal coefficient of the friction Fig. 9. In this case, the hard abrasive diamond medium greatly attenuated the signal relating to the coating as well as to the substrate by enabling a severe three-body abrasive wear mechanism to operate, leading to quicker wear and thus a very low coefficient of friction. However, under all of the load conditions, the FeSiNiCr coating demonstrated a significantly lower coefficient of friction than that pertaining to the substrate material. Appreciably hard abrasive particles, such as diamond, led to 'hard' abrasion.

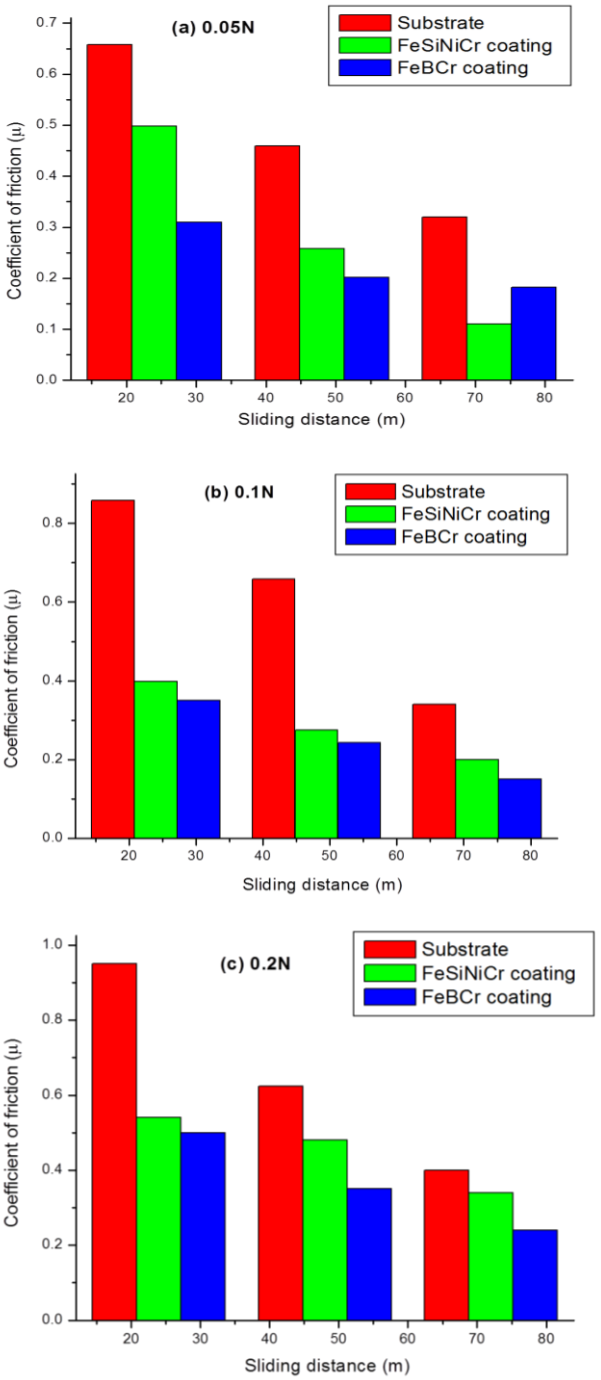

Fig. 9. Online monitoring of coefficient of friction for coating & substrate (a) 0.05 N, (b) 0.1 N, (c) 0.2 N.

The co-efficient of friction was measured on both the coated surfaces under dry sliding condition at different loads shown in the Fig. 9. It is observed that low co-efficient friction predicted in the both the coatings is much better in FeBCr coating compared with FeSiNiCr coating. FeBCr coated surface morphology showed fine grains present in the structure. It is in the monitoring of friction under dry sliding condition 0.05 N load applied, the FeSiNiCr coating co-efficient of friction is 20 % lower than

the substrate. The effect of the surface coating on the friction and wear Fig. 9, is low coefficient of friction compared to substrate materials.

3.6 SEM Micrograph of FeSiNiCr and FeBCr alloy coating wear morphology

In an attempt to establish the characteristics of the wear behaviour of the coatings, assessed after the use of different standardized test methods, the worn surfaces were examined by SEM. The wear scar nature of the tested coatings, assessed by SEM, Fig. 10, shows abrasive marks, pits and excess wear debris, indicating that three-body abrasive wear was the dominant wear mechanism. However, in addition, fine wear-tracks are observed uniformly all over the scar. Also, a few deep grooves are present, possibly formed due to the occurrence of ploughing during the test, caused by isolated and accumulated abrasive diamond particles. Under hard abrasion conditions, abrasive particles can cause plastic deformation in both the hard particles and the binder phase. The contact area for individual abrasive particles is usually much larger than that of the surface particle, and the wear occurs predominantly by plastic ploughing and cutting. Figure 10 shows the global distribution of wear debris. Signs of "adhesive wear" are also evident along the wear-tracks. SEM micrograph of FeBCr coating is shown in Fig. 10. From the examination of the wear scars from the FeBCr coating abraded with the diamond particle, two body abrasions are clearly observed. In the macro-scale mode, when the coating behaves homogeneously (like a solid material), plastic deformation occurs on the coated surface. The displacement and removal of material in this mode depends on the hardness of the coating. After abrasive wear testing, the worn surfaces of all samples were examined by SEM microscopy. Images of the central zone of the worn areas at the lowest and highest applied loads utilised were chosen and are shown in Fig. 10. The surfaces show evidence typical of rolling with significant indentation of the surface. In contrast, Figure shows evidence of typical of particle sliding (grooving) and also evidence typical of small particle rolling across the surface of the sample following abrasion with the diamond particles. The difference in wear mechanism between the crystalline coating and the substrate, the worn surfaces of FeBCr alloy coating were further examined by SEM. Light furrows and detached areas were observed on the worn surface of this coating, indicating that the wear was dominated by plastic deformation. However, the coating surface revealed that severe plastic deformation in the friction process, suggesting that adhesion was the dominant wear mechanism.

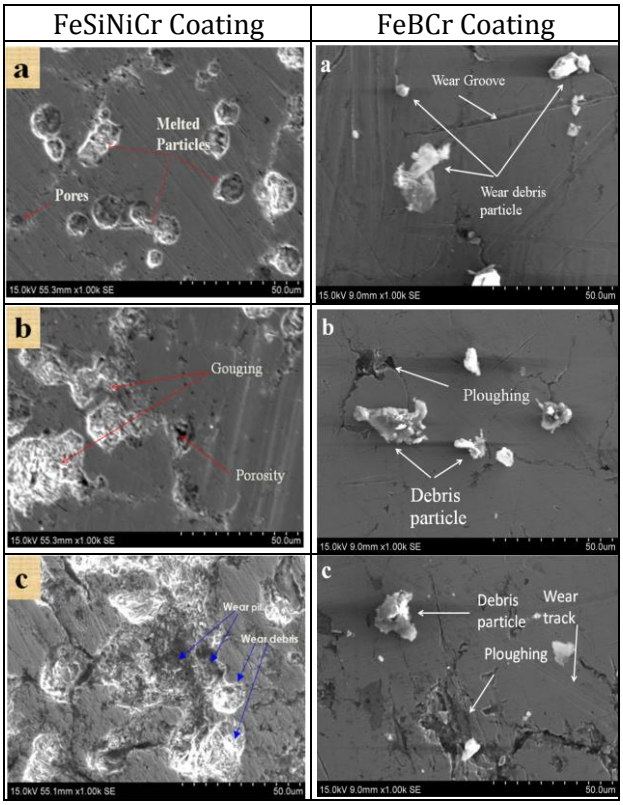

Fig. 10. SEM image shows abrasive wear particles debris from FeSiNiCr and FeBCr coated surface under condition (a) 0.05 N, (b) 0.1 N, (c) 0.2 N.

3.7 Weight loss measurement of FeSiNiCr and FeBCr coating

Figure 11 shows that the cumulative loss of material from coated specimen is due to the applied load in various conditions. The wear debris particles were removed from coated specimen at different time due to applied load. Normally the Fe based alloy coated specimen looses minimum debris particles during the test, because of the high hardness and fine dense layered coating deposited. The chart (Fig. 11) shows the weight loss during different duration of time for the three loads applied such as 0.05 N, 0.1 N and 0.2 N. It has been seen that the mass loss of the coating is lower than that of the substrate, indicating that coating has better resistance to wear resistance. Weight loss measurement for FeBCr coated materials at

different loading. Wear rate is obtained dividing the loss of volume [mm³] by the product of normal load applied and sliding distance. Mean values of the weight loss calculated at the end of the wear tests are reported in Fig. 11.

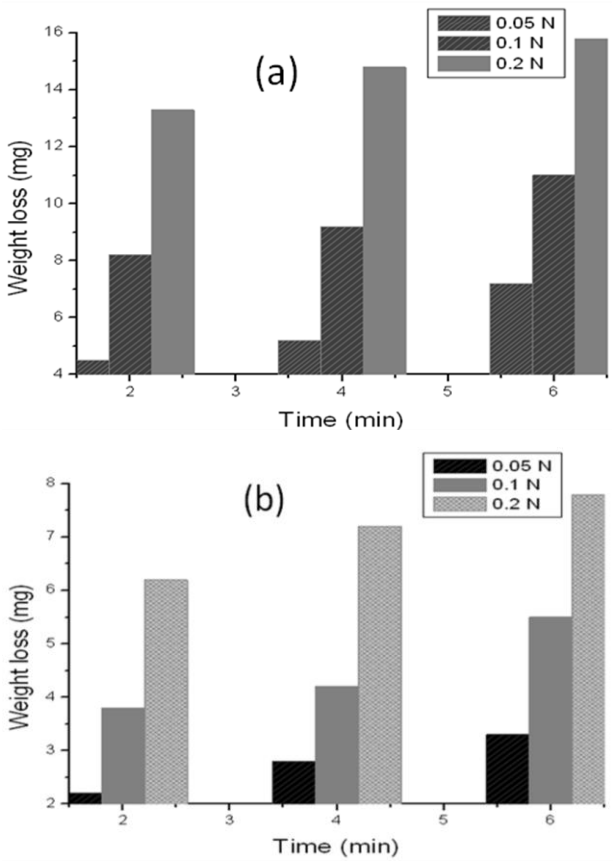

Fig. 11. Weight loss measurement of (a) FeSiNiCr coated specimen, (b) FeBCr coated specimen at ambient condition.

3.8 Corrosion behaviour of FeSiNiCr and FeBCr coated specimen

The chemical stability and the process involved in the corrosion of the metals were monitored by measuring the changes in OCP during immersion in electrolytic solution as a function of immersion time. Uncoated and coated substrates were immersed in 20 Wt.% H_2SO_4 solution for about 45 minutes and the changes in OCP for these substrates were recorded as a function of the immersion time. Relevant plots are given in Fig. 12. For the uncoated alloy, the observed potential was about -470 mV, with slight fluctuations, indicating the dissimilarities in potential at the different sites of the exposed surface in the corrosive medium. With the coated substrate, a 50 mV potential shift in the cathodic side was observed. In addition, the fluctuation was slightly greater than that of the uncoated substrate. This difference can be attributed to the existence of heterogeneities over the coated substrate. Potentiodynamic polarization studies of the uncoated substrate and of the Fe complex-based coated substrate, with the thickness of about 350 μm, were carried out using 20 Wt. % H_2SO_4 as the medium.

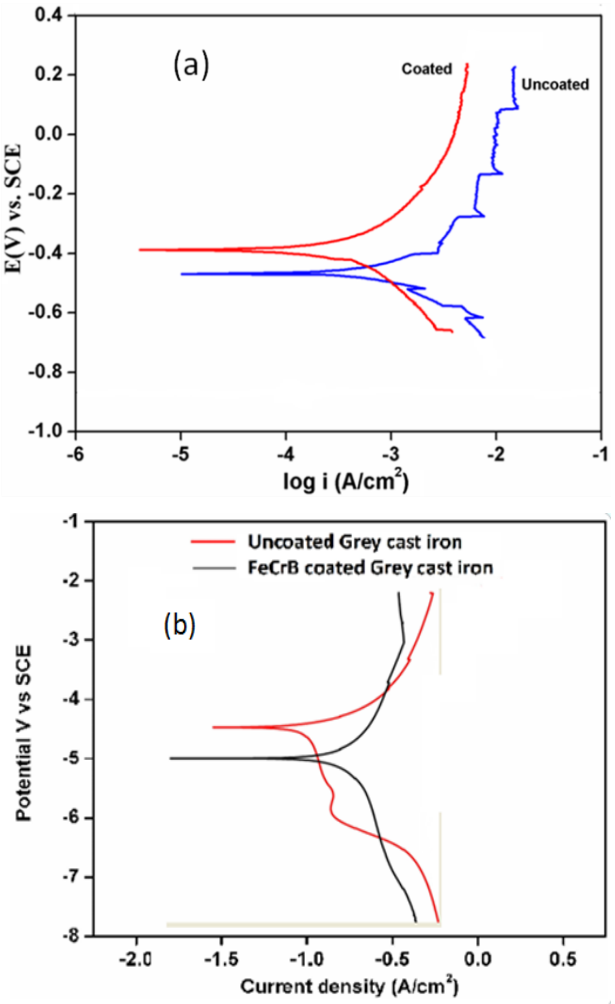

Fig. 12. Potentio dynamic polarization measurement of (a) FeSiNiCr coated specimen, (b) FeBCr coated specimen.

The observed polarization plots are given in Fig. 12. The corrosion current density (icorr) value obtained for the uncoated substrate was 3.0 mA/cm2. However, the corrosion current density (icorr) value that was obtained for the iron complex-coated substrate was 0.5 mA/cm2. It is seen from these results that the coated substrate gave a six time lower icorr value compared to the uncoated substrate. The lower icorr value that was obtained for the uncoated substrate indicates better corrosion resistance than the one which occurs with the

treated samples. The images of the coated specimen and of the uncoated specimen (Fig. 12) show that the corrosion products are not distributed uniformly.

In 0.5M H2SO4, the corrosion potential, Ecorr for the uncoated castiron material is −846 mV while that of the Fe59B26Cr15 alloy coated steel material is −931 mV. The coated steel has slightly lower corrosion potentials (Ecorr) than the uncoated steel. It is seen that the alloy, largely consisting of amorphous material has lower current densities than the crystalline alloy. The largely amorphous HVOF coating has lower current densities, i.e. better corrosion resistance, compared to the uncoated steel material. Corrosion current density, Icorr, values for both the un-treated and HVOF sprayed samples are approximately 0.1343 and 0.714 mA cm−2 respectively. There is a positive shift in Ecorr after the HVOF coating as shown in Fig. 12. Hence, the corrosion resistance is highly improved through FeCrB alloy coating.

4. CONCLUSIONS

FeSiNiCr and FeBCr coatings were successfully deposited by the HVOF spraying process to develop coatings of 350 to 400 μm in thickness on the Fe-based alloy substrates. From the detailed investigations, the following conclusions are drawn.The HVOF-sprayed coatings, with given parameters, have dense and uniform lamellar microstructures with porosities of less than 1.5 %. Further, a high proportion of the feedstock powders appeared to have been fully or partially melted prior to the impact on the substrate surface. The SEM micrographs indicate that both the coatings are free from surface/cross-sectional crack defects. SEM microstructure of FeSiNiCr coating showed the presence of graphite flakes; however, FeBCr coating showed splat like microstructure. X-ray diffractograms reveal that both FeSiNiCr powder alloy coatings and FeBCr powder alloy coatings exhibit BCC α-Fe matrix structure. The micro hardness of uncoated specimen was 380 HV; however, the micro hardness of the coated samples improved to 920 HV for FeSiNiCr coating and 980 HV for FeBCr coatings. The improvement in micro hardness values is due to low porosity accompanied by very fine grained microstructure. However, FeBCr coating exhibited superior hardness (6.5 % higher) compared to FeSiNiCr coating. The FeSiNiCr coatings exhibit excellent ability to resist localized corrosion when treated with 20 wt% H_2SO_4. It is noteworthy that coatings that have greater corrosion resistance than the substrate have been Also FeBCr coating has better corrosion resistance than FeSiNiCr alloy coating due to the presence of high chromium content and thus it is suitable for automotive applications.

REFERENCES

[1] K.W. Couch: *Studies of the flame spraying of polymers*, in: *Proceedings of the 9th national thermal spray conference*, Ohio, USA, pp. 251-255, 1996.

[2] A. Nakano, R. Kawase: *Production of heat and corrosion-resistant plastic coatings*, in: *Proceedings of the 9th National thermal spray conference*, Ohio, USA, pp. 257-262, 1996.

[3] J.A. Mareceau, A.A. Adjorlolo: *Commercial aircraft in ASTM, corrosion tests and standards application and interpretation*, American Society for Testing and Materials Society, pp. 574 -578, 1995.

[4] M. Seki, K. Ishikawa, S. Tobe: *Application of thermal spray coatings to prevent corrosion of construction in Japan*, in: *Proceedings of the 5th national thermal spray conference*, Anaheim, USA, pp. 679-684, 1993.

[5] L. Zhao: *Influence of the spraying processes on the properties of 316L stainless steel coatings*, Surface and Coatings Technology, Vol. 162, pp. 6-10, 2002.

[6] A.R. Nicoll: *Production plasma spraying in the automotive industry*, in: *A European View point: Proceedings of the 7th national thermal spray conference*, Boston, USA, pp. 7-17, 1994.

[7] Y. Wu, P. Lin, C. Chu, Z. Wang, M. Cao, J: *Cavitation erosion characteristics of a Fe–Cr–Si–B–Mn coating fabricated by high velocity oxy-fuel (HVOF) thermal spray*, Journal of Materials Letters, Vol. 61, No. 8-9, pp. 1867-1872, 2007.

[8] W. Fanga, T.Y. Choa, J.H. Yoona, K.O. Songa, S.K. Hura, S.J. Younb, H.G. Chun, HG: *Processing optimization, surface properties and wear behavior of HVOF spraying WC–CrC–Ni coating*, Journal of Materials Processing Technology, Vol. 209, No. 7, pp. 3561-3567, 2009.

[9] Y.P. Wu, P.H. Lin, Z.H. Wang, G.Y. Li: *Microstructure and microhardness characterization of a Fe-based coating deposited*

by high-velocity oxyfuel thermal spraying, Journal of Alloys and Compounds, Vol. 481, No. 1-2, pp. 719-724, 2009.

[10] N.F. Ak, C. Tekmen, I. Ozdemir, H.S. Soykan, E. Celik: *NiCr coatings on stainless steel by HVOF technique*, Surface and Coatings Technology, Vol. 173-174, No. 2, pp. 1070-1073, 2003.

[11] Hyung-Jun Kim, Stephanie Grossi & Young-Gak Kweon: *Wear performance of metamorphic alloy coatings*, Wear, Vol. 232, No. 1, pp. 51-60, 1999.

[12] S. Kuroda, Y. Tashiro, H. Yumoto, S. Taira, H. Fukanume, S. Tobe: *Peening action and residual stresses in high velocity oxygen fuel thermal spraying of 316L stainless steel*, Journal of Thermal Spray Technology, Vol. 10, No. 2, pp. 367-374, 2001.

[13] Z. Zhou, L. Wang, F.C. Wang, H.F. Zhang, Y.B. Liu, S.H. Xu: *Formation and corrosion behavior of Fe-based amorphous metallic coatings by HVOF thermal spraying*, Surface and Coatings Technology, Vol. 204, No. 5, pp. 563-570, 2009.

[14] F. Otsubo, A. Shimoda, H. Era, K. Kishitake: *Corrosion resistance of Fe-Cr-Mo-(C,B,P) amorphous coatings thermally sprayed by HVOF coating and APS processes*, in: *Proceedings of the international thermal spray conference,* Japan, pp. 439-441, 2004.

[15] M.S. Bakare, K.T. Voisey, K. Chokethawai, D.G. McCartney: *Corrosion behaviour of crystalline and amorphous forms of the glass forming alloy Fe43Cr16Mo16C15B10*, Journal of Alloys and Compounds, Vol. 527, pp. 210-218, 2012.

[16] S. Atamert, J. Stekly: *Microstruture, wear resistance, and stability of cobalt based and alternative iron based hard facing alloys*: Surface Engineering, Vol. 9, No. 3, pp. 231-240, 1993.

[17] J.A. Picas, Y. Xiong, M. Punset, L. Ajdelsztajn, A. Forna, J.M. Schoenung: *Microstructure and wear resistance of WC–Co by three consolidation processing techniques*, International Journal of Refractory Metals & Hard Materials, Vol. 27, pp. 344-349, 2009.

[18] M.S. Priyan, P. Hariharan: *Abrasive Wear Modes in Ball-Cratering Test Conducted on Fe73Si15Ni10Cr2 Alloy Deposited Specimen*, Tribology in Industry, Vol. 36, No. 1, pp. 97-106, 2014.

[19] M.S. Priyan, P. Hariharan, A. Azad, K.S. Kumar: *Microstructure and Wear Analysis of FeBCr Based Coating Deposited by HVOF Method*, Tribology in Industry, Vol. 36, No. 2, pp. 134-143, 2014.